

# RSC Advances

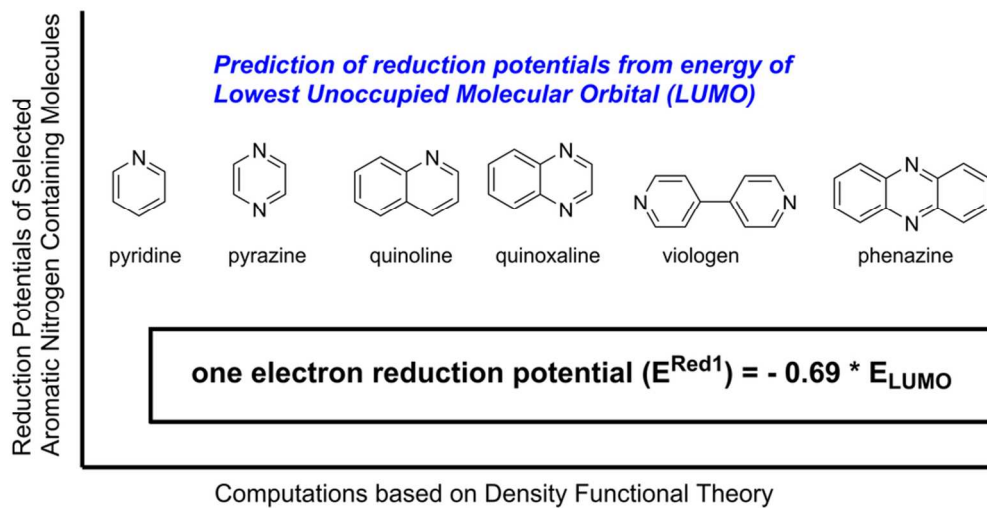


This is an *Accepted Manuscript*, which has been through the Royal Society of Chemistry peer review process and has been accepted for publication.

*Accepted Manuscripts* are published online shortly after acceptance, before technical editing, formatting and proof reading. Using this free service, authors can make their results available to the community, in citable form, before we publish the edited article. This *Accepted Manuscript* will be replaced by the edited, formatted and paginated article as soon as this is available.

You can find more information about *Accepted Manuscripts* in the [Information for Authors](#).

Please note that technical editing may introduce minor changes to the text and/or graphics, which may alter content. The journal's standard [Terms & Conditions](#) and the [Ethical guidelines](#) still apply. In no event shall the Royal Society of Chemistry be held responsible for any errors or omissions in this *Accepted Manuscript* or any consequences arising from the use of any information it contains.



A descriptive relationship for computing reduction potentials of selected aromatic nitrogen containing molecules is developed from their computed orbital energies  
86x43mm (300 x 300 DPI)

## Reduction Potential Prediction of Some Aromatic Nitrogen Containing Molecules

Rajeev S. Assary<sup>1,2,\*</sup>, Fikile R. Brushett<sup>1,3</sup>, Larry A. Curtiss<sup>1,2</sup>

<sup>1</sup> Joint Center for Energy Storage Research, Argonne National Laboratories, Argonne, IL, 60439

<sup>2</sup> Materials Science Division, Argonne National Laboratory, Argonne, IL, 60439

<sup>3</sup> Department of Chemical Engineering, Massachusetts Institute of Technology, Cambridge, MA, 02139

Keywords: *non-aqueous redox flow battery, quinoxaline, density functional theory, reduction potentials*

Corresponding author: RSA ([assary@anl.gov](mailto:assary@anl.gov)), Phone: 001-630-252-3536, Fax 630-252-9555

## Abstract

Accurate quantum chemical methods offer a reliable alternative to time-consuming experimental evaluations for obtaining *a priori* electrochemical knowledge of a large number of redox active molecules. In this contribution, quantum chemical calculations are performed to investigate the redox behavior of quinoxalines, a promising family of active materials for non-aqueous flow batteries, as a function of substituent group. The reduction potentials of 40 quinoxaline derivatives with a range of electron-donating and electron-withdrawing groups are computed. Calculations indicate the addition of electron-donating groups, particularly alkyl groups, can significantly lower the reduction potential albeit with a concomitant decrease in oxidative stability. A simple descriptor is derived for computing reduction potentials of quinoxaline derivatives from the LUMO energies of the neutral molecules without time-consuming free energy calculations. The relationship was validated for a broader set of aromatic nitrogen-containing molecules including pyrazine, phenazine, viologen, pyridine, pyrimidine, pyridazine, and quinoline, suggesting that it is a good starting point for large high-throughput computations to screen reduction windows of novel molecules.

## 1. INTRODUCTION

Fundamental breakthroughs are required in electrochemical systems such as advanced metal-intercalation, metal/air, metal/sulfur, and redox flow batteries to improve efficient energy storage for transportation and stationary needs<sup>1-7</sup>. A redox flow battery (RFB) is an electrochemical device that stores energy in flowable solutions, or suspensions, of electroactive materials, which are housed in external tanks and pumped to a power-generating electroreactor<sup>8,9</sup>. As compared to enclosed rechargeable batteries, RFBs may offer a number of advantages in terms of cost, performance, and flexibility including decoupled power and energy, long operating lifetimes, simplified manufacturing, and improved safety.

Recently, RFBs based on sustainable organic redox materials have drawn attention as one of the promising candidates due to its potential to operate in large electrochemical window, with low cost, and high solubility<sup>9-16</sup>. For example, Aziz et al.<sup>13</sup> and Narayan et al.<sup>14</sup> have reported the use of quinone derivatives in acidic aqueous RFBs. Under non-aqueous conditions, molecules such as anthraquinone<sup>13, 17, 18</sup>, quinoxaline<sup>11</sup>, and thiophene<sup>19,20</sup> have been investigated for energy storage applications. Moreover, a number of high potential redox shuttles have been developed for overcharge protection in lithium-ion batteries<sup>21</sup>. Recently, Brushett et al. demonstrated an all-organic non-aqueous redox flow battery (NRF) based on quinoxaline derivatives and 2,5-di-tert-butyl-1,4-bis(2-methoxyethoxy)benzene (DBBB, also referred to as ANL RS2)<sup>11</sup>.

There are a large number of redox active organic molecules (e.g., aromatics containing N, S, and O atoms) that may be considered for use in NRF batteries. Consequently, the identification of optimal redox couples via experimentation is a daunting task and rapid screening of redox properties via reliable computational methods represents a powerful means of down selecting candidates with minimal investment. Indeed, employing accurate quantum

chemical methods may allow the screening of thousands of molecules for desired electrochemical window, solubility, and stability. Quantum chemical studies to understand the electrochemical windows of selected chemical families such as hydrocarbons<sup>22</sup>, quinones<sup>23-28</sup> and isoindoles<sup>29,30</sup> are available in the literature. These studies provide basic understanding of the electrochemical windows that can be used as a first level of screening approach to narrow down a large molecular set. Similar ‘genome’ scale approaches were found to be efficient for materials discovery for battery<sup>31,32</sup> and photovoltaic applications<sup>33</sup>.

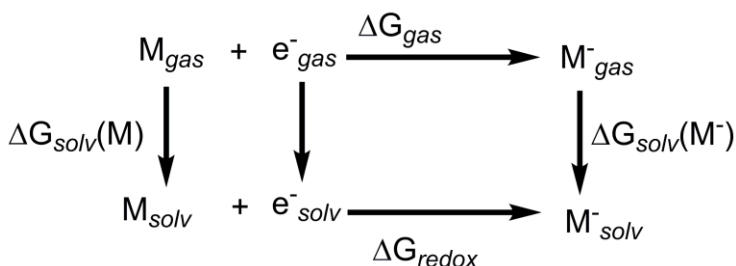
Herein, we use computations based on density functional theory (DFT) to investigate reduction potentials of quinoxaline and a number of derivatives (40 molecules) as negative electrolyte materials for NRF batteries (Scheme S1)<sup>11</sup>. First, we modeled the impact of electron-donating and electron withdrawing substituent groups on the reduction potentials of quinoxaline molecules. Second, we use the data generated to derive an empirical relationship that connects reduction potentials with energies of lowest unoccupied molecular orbitals (LUMOs). Third, we extended this relationship to other aromatic nitrogen containing molecules (40 molecules) including pyrazine, phenazine, and viologen derivatives. These simple descriptors may be used in high throughput computational screening of thousands of organic molecules to down select candidates with promising reduction properties for RFB application.

## 2. METHODS

### 2.1 Computational Details

All calculations presented in the paper are performed using the Gaussian 09 software<sup>34</sup>. The B3LYP/6-31+G(d) level of theory is used to compute the structure and energetics of all species in the gas phase. The same level of theory was used to calculate zero point energies, free energy corrections (298 K, 1 atm pressure) and solvation energies. The SMD<sup>35</sup> model was used

to compute the solvation free energy by a single point energy calculation on the gas phase optimized geometry using water as the dielectric medium<sup>35</sup>. We find that this is an effective approximation for computing free energies of redox active species in solution and this level of theory is reasonably accurate for the computation of reduction potentials (see Table S1A of the supporting information for the benchmarking of the accuracy of density functional methods). We have optimized selected systems using the SMD solvent (water dielectric medium) model to include the solvation effects in determining the geometry and energy. For this study, changing the dielectric medium to acetone, dimethyl sulfoxide, or methanol did not significantly impact the computed redox potentials of quinoxaline derivatives (see Table S1B of the supporting information). The Gibbs free energy of molecule ‘M’ in the solution is computed as the sum of the free energy in the gas phase ( $G_{gas}$ ) and the solvation free energy ( $\Delta G_{solv}$ ).



**Scheme 1.** Thermodynamic cycle involved in the reduction process of molecule M.

Using the thermodynamic cycle shown Scheme 1, solution phase free energy change for reduction or oxidation process ( $\Delta G_{redox}$ ) can be computed as:

$$\Delta G_{redox} = \Delta G_{gas} + \Delta \Delta G_{solv} \quad \text{Eq. 1,}$$

Where  $\Delta \Delta G$  is:

$$\Delta \Delta G = \Delta G_{solv}(M^-) - \Delta G_{solv}(M) \quad \text{Eq.2,}$$

where the change in energy of electrons when going from vacuum to non-aqueous solution

( $e^-_{(gas)} \rightarrow e^-_{(solv)}$ ) is approximated as zero since it is negligibly small (0.03 eV<sup>36</sup>), similar to recent

studies<sup>37, 38</sup>. From the Gibbs free energy ( $\Delta G_{redox}$ ), the redox potential with respect to Li/Li<sup>+</sup> ( $E_{redox}^V$ ) can be calculated using the following equation:

$$E_{redox}^V = \frac{-\Delta G_{redox}}{nF} - 1.24 \quad \text{Eq. 3,}$$

where  $n$  is the number of electrons involved in the redox reaction and  $F$  is the Faraday constant. The constant '-1.24 V' represents the difference between the standard hydrogen electrode (SHE, -4.28 V<sup>39</sup>) and Li/Li<sup>+</sup> redox couple (-3.04 V) and is required to convert the free energy changes to reduction potential with respect to Li/Li<sup>+</sup> reference electrode, a commonly used experimental convention<sup>38, 40, 41</sup>. Further details regarding the computation of redox potential can be found elsewhere<sup>28, 36, 37, 42-48</sup>.

Additionally it should be noted that the binding of second electron to the mono-anion in the gas phase is thermodynamically uphill (negative electron affinity), while inclusion of solvation contributions favors the binding of the second electron. The negative electron affinities result in less accurate reduction potential, but in cases where experimental values are available agreement is reasonable. It has been found that finite basis sets can give reasonable results in comparison to gas phase experimental results for gas phase temporary anions with negative electron affinities due to a cancellation of errors<sup>49</sup>. In general, quantum chemical calculations can be used to compute the redox potentials of a material of interest with reasonable accuracy<sup>28, 48, 50, 51</sup>.

### 3. Results and Discussions

#### 3.1 The Impact of Substituent Groups on Calculated Redox Potentials and Specific Energy

As quinoxalines are predominantly under investigation for negative active species, our focus will be to determine how to most effectively lower the reduction potential without significantly increasing the molecular weight (thus lowering the charge storage capacity). Figure 1 shows the

computed highest occupied molecular orbital (HOMO) and lowest unoccupied molecular orbital (LUMO) for unsubstituted quinoxaline. The HOMO is located in the benzene ring, while the LUMO is located in the pyrazine ring of the quinoxaline. Note that the computed oxidation potential of unsubstituted quinoxaline is 5.26 V due to the stability of HOMO orbital, consistent with the oxidative stability of benzene. From the computed LUMO of quinoxaline, it is clear that the nitrogen containing ring is responsible for the electron affinity of quinoxaline and, therefore, the reduction potential of quinoxaline and its derivatives can be most effectively altered by substitution on this ring.

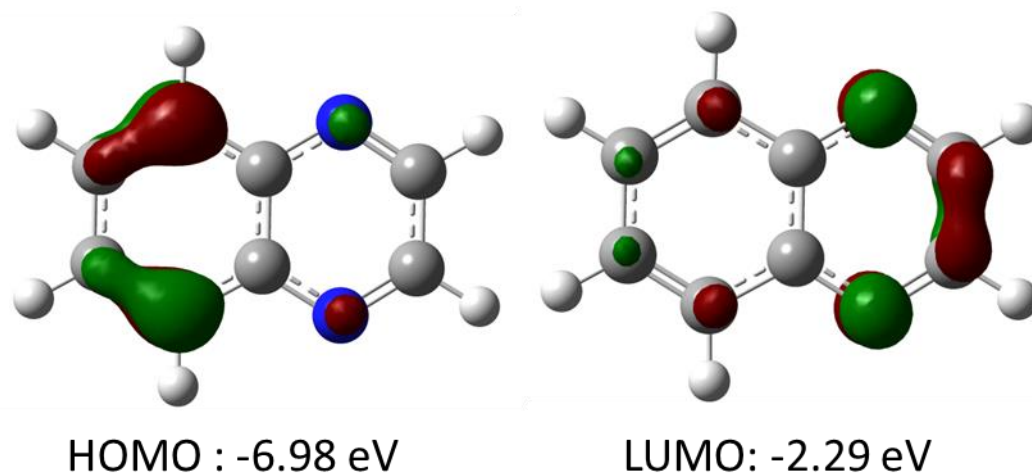


**Figure 1.** Computed molecular orbitals HOMO and LUMO of quinoxaline.

To explore the effect of substitutions on reduction potential, oxidation potential, and specific energy (normalized to a common reference), 40 quinoxaline derivatives are investigated (Figure 2).

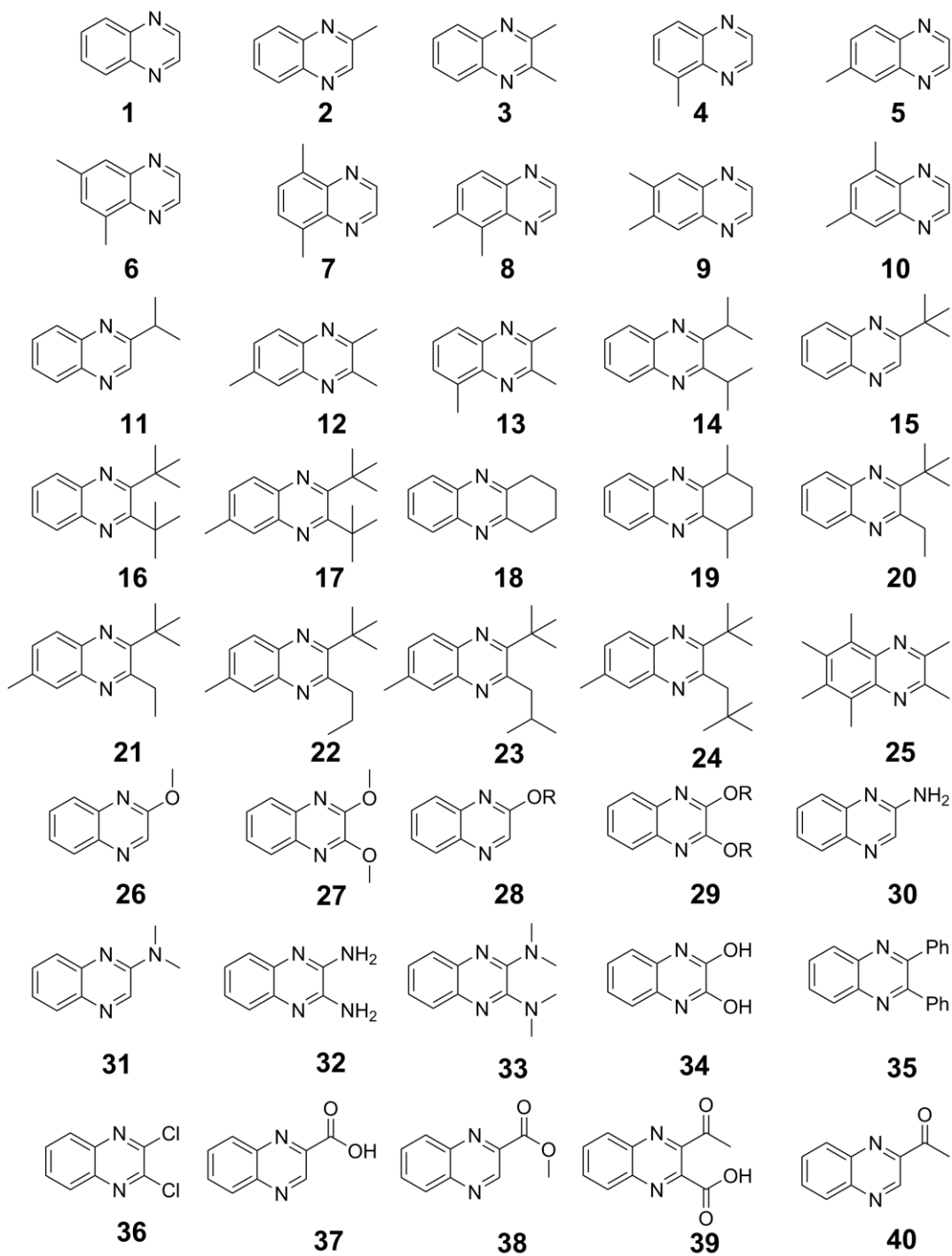


Figure 2. Selected quinoxaline derivatives, where entry 1 is unsubstituted quinoxaline

**Table 1.** Computed LUMO energies (eV), first electron reduction ( $\Delta E^{\text{Red1}}$ ), second electron reduction ( $\Delta E^{\text{Red2}}$ ), first oxidation ( $\Delta E^{\text{Ox1}}$ ) potentials, predicted reduction potentials and error function of quinoxaline derivatives (entries 1 to 40, shown in Figure 2). The reduction / oxidation potentials are computed at the B3LYP/6-31+G(d) level of theory. Negative of LUMO energies is tabulated as the electron affinity (EA). Italicized values in parenthesis are from previous experimental studies. <sup>a</sup> Details of predicted first reduction potentials and error function are shown in Section 3.2.

Entries (as shown in Fig. 2)	Electron affinity	Potential vs. Li/Li <sup>+</sup> (V)				
	(-ve of LUMO)	E <sup>Red1</sup> computed from Eq. 3			<sup>a</sup> Predicted reduction potential = (0.69* EA)	<sup>a</sup> Error function
	EA (eV)	E <sup>Red1</sup>	E <sup>Red2</sup>	E <sup>Ox1</sup>	*E <sup>Red1</sup>	$\delta E = (*E^{\text{Red1}} - E^{\text{Red1}})$
1	2.29	1.55 ( <i>1.52</i> <sup>52</sup> )	1.00	5.26	1.58	0.03
2	2.10	1.44	0.89	5.14	1.45	0.01
3	1.94	1.34 ( <i>1.45</i> <sup>52</sup> )	0.83	5.06	1.34	0.00
4	2.21	1.49	0.91	4.90	1.53	0.04
5	2.21	1.53	0.89	4.97	1.53	0.00
6	2.10	1.44	0.85	4.74	1.45	0.01
7	2.15	1.44	0.93	4.63	1.48	0.04
8	2.12	1.43	0.84	4.71	1.46	0.03
9	2.08	1.45	0.81	4.89	1.44	-0.01
10	2.14	1.48	0.88	4.70	1.48	0.00
11	2.08	1.36	0.85	5.06	1.44	0.08
12	1.84	1.3	0.77	4.86	1.27	-0.03
13	1.89	1.29	0.73	4.76	1.30	0.01
14	1.98	1.33	0.76	4.91	1.37	0.04
15	2.05	1.31	0.85	5.03	1.42	0.11
16	1.92	1.25	0.69	4.66	1.32	0.07
17	1.82	1.18	0.63	4.57	1.25	0.07
18	1.95	1.36	0.74	5.01	1.35	-0.01
19	1.90	1.24	0.67	4.91	1.31	0.07
20	1.89	1.31	0.75	4.83	1.31	0.00
21	1.79	1.25	0.69	4.77	1.24	-0.01
22	1.83	1.21	0.66	4.79	1.26	0.05
23	1.86	1.2	0.66	4.69	1.28	0.08
24	1.87	1.19	0.63	4.69	1.29	0.10
25	1.64	1.14	0.49	4.27	1.13	-0.01
26	2.00	1.36	0.86	5.06	1.38	0.02
27	1.83	1.46	0.87	4.73	1.27	-0.19
28	2.10	1.43	0.89	5.15	1.45	0.02
29	1.98	1.65	0.93	5.16	1.36	-0.29
30	1.91	1.28	0.75	4.40	1.32	0.04
31	1.79	1.24	0.75	4.06	1.23	-0.01
32	1.58	1.03	0.59	4.06	1.09	0.06
33	1.52	1.18	0.63	4.57	1.05	-0.13
34	1.96	1.31	0.77	4.96	1.35	0.04
35	2.23	1.55 ( <i>1.77</i> <sup>52</sup> )	1.09	4.73	1.54	-0.01
36	2.70	1.78	1.35	5.58	1.86	0.08
37	2.82	2.08	1.62	5.48	1.95	-0.13
38	2.68	2.01	1.53	5.46	1.85	-0.16
39	2.65	2.15	1.67	5.61	1.83	-0.32
40	2.82	2.07	1.60	5.29	1.95	-0.12

The set of entries can be partitioned into the following substituent groups: alkyl groups (electron donating, entries 2 – 25), alkoxy groups (electron donating, entries 25 – 29), amino and hydroxyl groups (electron donating, entries 30 – 34), and phenyl, chloro, acetyl, and ester groups (electron withdrawing, entries 35 – 40). Based on the HOMO and LUMO characteristics of unsubstituted quinoxaline (Figure 1), the introduction of electron donating groups in the nitrogen ring increases the electron density and, hence, decreases the electron affinity and reduction potential. Where possible, the computed reduction potentials of quinoxaline derivatives are compared to experimentally-obtained values to determine model accuracy and validate trends. It is important to note that, in this study, explicit effects of salts, impurities, concentration, and electrode materials are not considered, which may be significant for comparison with experiments.

Ames *et al.* reported the quinoxaline reduction at -1.8 V vs. SCE (ca. 1.50 V vs. Li/Li<sup>+</sup>) in 0.1 M TEAP in dimethylformamide.<sup>52</sup> Similarly, Barqawi and Atfah reported -1.62 V vs. SCE (ca. 1.7 V vs. Li/Li<sup>+</sup>) in 0.1 M TBAPF<sub>6</sub> in acetonitrile.<sup>53</sup> The computed reduction potential of quinoxaline is 1.55 V vs. Li/Li<sup>+</sup> (Table 1, entry 1) is reasonably consistent with the experiments indicating the reliability of the computational methods used here. The computed potentials of alkyl-substituted quinoxalines (entries 2 to 25) clearly show a lowering in the reduction potentials. The most effective positions for methyl/alkyl substitutions are positions 2 and 3 of the quinoxaline. Among alkyl substituted quinoxalines, entries 3, 11, 12, 13, 14 and 15 appear the most promising candidates in terms of the electrochemical window, with minimal substitutions (important for maximizing molecular capacity). From quinoxaline (entry 1) to 2,3,5,6,7,8-hexamethyl quinoxaline (entry 25), a decrease of reduction potential by 0.41 V for the first reduction event is computed, which is the maximum decrease computed for alkyl substitutions

among our data set. The computed potential in the second electron transfer process of that same species 25 is 0.51 V less than that of quinoxaline. However, concomitant with the decrease in reduction potential is a decrease in the oxidative stability of this species of almost 1 V as compared to quinoxaline (5.26 V). This may be acceptable as the negative electrolyte would not be expected to reach those potentials. The introduction of alkoxy groups (entries 27 to 29) in either position 2 or 3 of quinoxaline shows less significant impact on redox potentials as compared to alkyl groups. Further, the introduction of other electron-donating groups such as amino (entries 30 & 32) or dimethyl amino groups (entries 31 & 33) also results in a decrease of the redox potential, albeit less effective than the addition of alkyl groups.

Electron withdrawing groups increase the electron affinity and hence increase the redox potential (entries 36 to 40). For instance, the computed reduction potential of 2,3-dichloroquinoxaline (entry 36) is 0.23 V higher than that of unsubstituted quinoxaline. Similarly, functional groups such as carboxyl (entry 37), ester (entries 38 & 39), and acetoxy (entry 40) increases the reduction potential by ~0.5 V for both first and second electron reduction process. Note that chloro-substituted quinoxaline (entry 36) is not stable upon the second reduction, where detachment of C-Cl bond occurs. The C-Cl bond length increases from 1.75 Å (neutral) to 1.79 Å (singly reduced) and subsequently to 1.96 Å (doubly reduced) suggesting that decomposition is likely during the reduction process. For substituents that contains C=O group (acetyl group), major structural changes occur in the C=O group rather than the quinoxaline ring resulting in different redox characteristics than the quinoxaline or its methylated counterparts.

**Table 2.** Computed energy densities of quinoxaline derivatives (entries 1 to 40, shown in Figure 2) normalized against unsubstituted quinoxaline (Q) is shown. Using DBBB-based positive electrolyte (ca. 4 V vs. Li/Li<sup>+</sup>) as a reference point, the change in specific energy for each derivative is calculated and normalized to quinoxaline.

Entries	Specific Energy Evaluation					
	Molecular weight	Number of electrons	Mol. Cap.= <i>MC</i> (Ah/kg)	Average Redox Voltage (V)	Specific Energy ( <i>SE</i> )(vs. DBBB) (Wh/kg)	Normalized Specific Energy vs. Quinoxaline(Q)
	MW (g/mol)	<i>n</i>	<i>MC</i> = <i>nF</i> /MW	<i>V</i> = ( <i>E</i> <sup>Red1</sup> + <i>E</i> <sup>Red2</sup> )/ <i>n</i>	<i>SE</i> = <i>MC</i> (4- <i>V</i> )	<i>SE</i> [i]/ <i>SE</i> [Q]
1 (Q)	130.15	2	411.86	1.28	1122.31	1.00
2	144.17	2	371.80	1.17	1054.06	0.94
3	158.2	2	338.83	1.09	987.69	0.88
4	144.17	2	371.80	1.20	1041.05	0.93
5	144.17	2	371.80	1.21	1037.33	0.92
6	158.2	2	338.83	1.15	967.36	0.86
7	158.2	2	338.83	1.19	953.81	0.85
8	158.2	2	338.83	1.14	970.75	0.86
9	158.2	2	338.83	1.13	972.44	0.87
10	158.2	2	338.83	1.18	955.50	0.85
11	172.33	2	311.05	1.12	895.82	0.80
12	172.33	2	311.05	1.04	922.26	0.82
13	172.33	2	311.05	1.01	930.03	0.83
14	214.31	2	250.12	1.05	739.10	0.66
15	186.25	2	287.80	1.04	851.89	0.76
16	242.36	2	221.17	0.97	670.15	0.60
17	256.39	2	209.07	0.91	647.07	0.58
18	184.24	2	290.94	1.05	858.28	0.76
19	212.29	2	252.50	0.94	772.65	0.69
20	214.31	2	250.12	1.03	742.85	0.66
21	228.33	2	234.76	0.97	711.33	0.63
22	242.26	2	221.26	0.94	678.17	0.60
23	256.39	2	209.07	0.93	641.84	0.57
24	270.41	2	198.23	0.91	612.53	0.55
25	214.31	2	250.12	0.82	796.63	0.71
26	160.17	2	334.66	1.11	967.18	0.86
27	190.2	2	281.82	1.17	798.97	0.71
28	145.14	2	369.32	1.16	1048.87	0.93
29	160.13	2	334.75	1.29	907.16	0.81
30	145.16	2	369.27	1.02	1102.27	0.98
31	173.21	2	309.47	1.00	929.95	0.83
32	160.18	2	334.64	0.81	1067.51	0.95
33	216.28	2	247.84	0.91	767.07	0.68
34	162.15	2	330.58	1.04	978.51	0.87
35	282.34	2	189.85	1.32	508.80	0.45
36	199.34	2	268.90	1.57	654.78	0.58
37	174.16	2	307.78	1.85	661.73	0.59
38	188.18	2	284.85	1.77	635.21	0.57
39	246.22	2	217.70	1.91	455.00	0.41
40	172.18	2	311.32	1.84	674.01	0.60

Using 4 V vs. Li/Li<sup>+</sup> as a common reference point (redox potential of DBBB-based positive electrolyte), a high-level specific energy calculation performed for each of the 40 quinoxaline derivatives and then normalized to unsubstituted quinoxaline (Q, entry 1 in Table 2). For this particular data set, none of the voltage changes offset the increase in molecular weight meaning that the specific energy of all the substituted quinoxaline derivatives was lower than the unsubstituted quinoxaline. However, it is important to note that these candidates represent only a small subset of the possible quinoxaline derivatives and that the addition of substituent groups can impart other favorable properties (e.g., solubility, diffusivity, viscosity) beyond modifying reduction potential.

### 3.2 A Descriptor for Reduction Potential Evaluation for Quinoxaline Derivatives

Data presented in Table 1 represent a small fraction of the possible quinoxaline derivatives that may be utilized as charge storage species. However, though faster than manual synthesis and experimentation, mapping thousands of redox candidates via free energy calculations is time-consuming and limits throughput. Developing simple high-level descriptors to predict redox windows can significantly accelerate the innovation process. Indeed, similar approaches have been successfully employed for the high throughput calculation of battery and photovoltaic materials<sup>13, 32, 33</sup>. Thus linking the reduction potential evaluation presented in the previous section to a larger set of quinoxaline derivatives, requires simple descriptors to predict reduction potential. Using the first reduction potential data of quinoxaline derivatives (entries 1 to 40 shown in Table 1), it is possible to derive a simple descriptor that enables the prediction of first reduction potentials of novel quinoxaline derivatives. According to the Nernst relation (Eq. 3), the computed reduction potential ( $E_n^{redI}$ ) of a quinoxaline derivative  $n$  (denoted entry  $n$ ) is directly proportional to the free energy change associated with the reduction process ( $\Delta G_n^{redI}$ ),

which, in turn is proportional to the electron affinity ( $EA$ ) of the molecule. The electron affinity ( $EA$ ) of the molecule is directly proportional to the LUMO energy ( $\epsilon_{LUMO}$ ) of the molecule (Eq. 4).

$$\Delta G_n^{red1} = k_1 EA \quad \text{Eq. 4}$$

$$EA = k_2 \epsilon_{LUMO} \quad \text{Eq. 5}$$

Where  $k_1$  and  $k_2$  in Eq.4 and 5 are constants.

Using Eq. 3 and 4, the reduction potential ( $E_n^{red1}$ ) can be written using the following equation;

$$E_n^{red1} = -k_1 k_2 * \epsilon_{LUMO} \quad \text{Eq. 6}$$

$$E_n^{red1} = -K_n * \epsilon_{LUMO} \quad \text{Eq. 7}$$

Where  $K_n$  is the product of  $k_1$  and  $k_2$ .

As part of the data set developed for the 40 quinoxaline derivatives shown in Table 1, we have computed the ' $K_n$ ' (for  $n = 1$  to 40) values using the computed reduction potentials and energy of the LUMO. The computed average value of  $K_n$  is 0.69. Therefore, the prediction of the first reduction potential of a new quinoxaline derivative can be made using the following relationship, upon computing the LUMO energy ( $\epsilon_{LUMO}$ ) of the neutral molecule.

$$E_{novel}^{red1} = -0.69 * \epsilon_{LUMO} \quad \text{Eq. 8}$$

To show this comparison more effectively, we have computed the error function ( $\delta E$ ), a difference between the predicted reduction potentials ( $*E^{Red1}$ ) using the Eq. 8 and the computed reduction potentials ( $E^{Red1}$ ) from the Eq. 3 (Nernst equation) are evaluated and shown in Table 1. The predicted reduction potentials are consistent with that of the computed reduction potentials as shown Table 1 and Figure S1 average deviation between computed vs. predicted reduction potentials is 0.07 V. The greatest advantage of predicted potential over the computed one is the

simplicity of the former, where, only a single point energy evaluation of the neutral species is essential while the latter require more computationally-intensive free energy evaluations of the neutral and anions in solution. We note that, using scaled LUMO energies it is possible to predict the electron affinity of organic molecules with reasonable accuracy<sup>54</sup>, unless the LUMO orbital of the molecule is poorly defined by the level of theory<sup>55</sup>. Additionally, the redox window is one of the desired properties required for screening. Other descriptors for solubility and stability are required for screening and to narrow down the candidates. This will be subject for further investigation.

### 3.3 Validation of reduction potential descriptors for other nitrogen-containing species

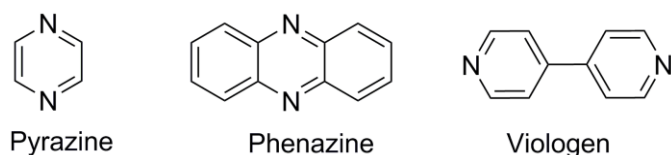


**Figure 3.** Schematic representation of pyrazine, phenazine, and viologen molecules

In the previous section, we have successfully developed and tested a descriptive relationship for evaluating reduction potentials of a quinoxaline derivatives using computed LUMO energy of neutral species. To assess the broad applicability of this descriptive relationship for predicting reduction potential of selected other nitrogen-containing redox active molecules including pyrazine, phenazine, and viologen families (shown in Figure S2a, b, c, respectively). The computed LUMO energies (eV), predicted first reduction potentials ( $*E^{Red1}$ ) using Eq. 8, and computed reduction potentials ( $E^{Red1}$ ) using Eq. 3 for these 40 molecules are presented in Table 3. The computed first reduction potential of pyrazine, phenazine, and

viologen are in good agreement ( $\pm 0.1$  V) with experimental studies<sup>56-58</sup> (Table 3) indicating the accuracy of the computation methods.

**Table 3.** Computed LUMO energies (eV), predicted first reduction potentials ( $*E^{\text{Red1}}$ ), and computed reduction ( $E^{\text{Red1}}$ ) of pyrazine (P), phenazine (Ph), and viologen (V) derivatives at the B3LYP/6-31+G(d) level of theory.

Entries <sup>a</sup>	Molecular Species	LUMO (eV)	reduction potentials (V vs. Li/Li <sup>+</sup> )	
			Predicted	Computed
			$*E^{\text{Red1}}$	$E^{\text{Red1}}$
41	pyrazine (P)	-1.83	1.07	1.10 ( <i>1.12</i> <sup>56</sup> )
42	2-methyl P	-1.62	0.95	0.97
43	2,3-dimethyl P	-1.44	0.84	0.82
44	2,5-dimethyl P	-1.45	0.85	1.01
45	2,6-dimethyl P	-1.50	0.88	0.96
46	2,3,5-trimethyl P	-1.27	0.74	0.84
47	2,3,5,6-tetramethyl P	-1.12	0.65	0.69
48	2-methoxy P	-1.58	0.92	1.02
49	2,3-dimethoxy P	-1.13	0.66	0.69
50	2,5-dimethoxy P	-1.53	0.89	1.02
51	2,6-dimethoxy P	-1.24	0.72	0.75
52	2,3,5,6-tetramethoxy P	-0.81	0.47	0.66
53	phenazine (Ph)	-2.75	1.90	2.01 ( <i>2.04</i> <sup>57</sup> )
54	1-methyl Ph	-2.69	1.85	1.96
55	2-methyl Ph	-2.85	1.97	1.98
56	1,2dimethyl Ph	-2.62	1.81	1.95
57	1,3-dimethyl Ph	-2.58	1.78	1.88
58	1,4-dimethyl Ph	-2.62	1.81	1.91
59	1,2,3-trimethyl Ph	-2.53	1.74	1.86
60	1,2,3,4-tetramethyl Ph	-2.45	1.69	1.99
61	2,3-dimethyl Ph	-2.57	1.77	1.91
62	1-chloro Ph	-2.95	2.04	2.13
63	2-chloro-Ph	-2.95	2.04	2.11
64	1,2,8,9-tetramethyl Ph	-2.49	1.72	1.84
65	1,4,6,9-tetramethyl Ph	-2.43	1.67	1.74
66	1,2,7,8-tetramethyl Ph	-2.46	1.70	1.81
67	1,2,6,7-tetramethyl Ph	-2.45	1.69	1.78
68	2,3,7,8-tetramethyl Ph	-2.40	1.65	1.8
69	1,2,3,4,6,7,8,9-octamethyl Ph	-2.18	1.51	1.57
70	1-tertbutyl Ph	-2.68	1.85	1.9
71	2-tertbutyl Ph	-2.67	1.84	1.96
72	viologen (V)	-2.02	1.18	1.31 ( <i>1.19</i> <sup>58</sup> )
73	2-methyl V	-1.94	1.13	1.27
74	2,3-dimethyl V	-1.62	0.94	1.00
75	2,5-dimethyl V	-1.70	0.99	1.05
76	2,6-dimethyl V	-1.87	1.09	1.21
77	2,3,5,6-tetramethyl V	-1.17	0.69	0.70
78	2,2'-dimethyl V	-1.86	1.09	1.21
79	2,2',6,6'-tetramethyl V	-1.72	1.00	1.15
80	2,2',3,3',5,5',6,6'-octamethyl V	-0.63	0.37	0.32

Italicized values in parenthesis are from previous experimental studies. <sup>a</sup> Schematic of all the structures are given in Fig. S2.

From the Table 3, it is shown that the predicted reduction potentials are in good agreement with the computed reduction potentials (from thermodynamic cycle).

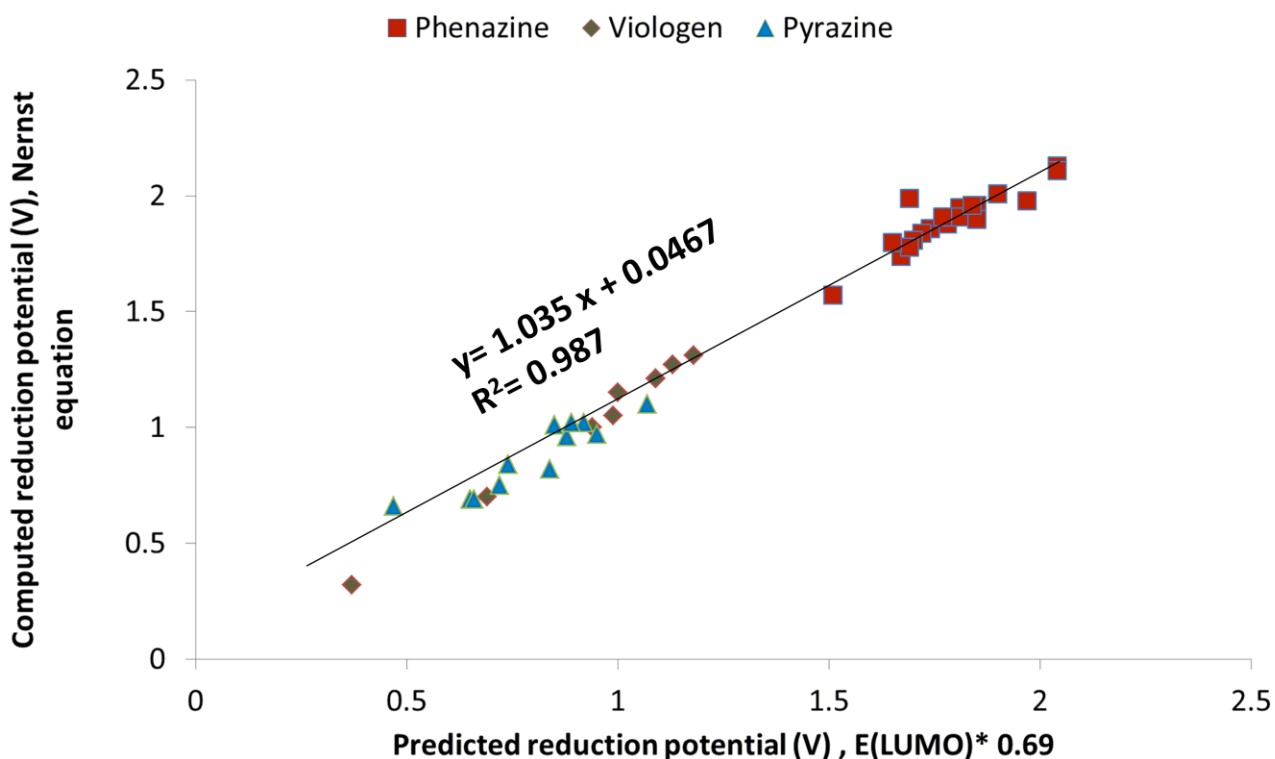


**Figure 4.** Computed reduction potentials using Eq. 3 vs. the predicted reduction potential using Eq. 8 for pyrazine, phenazine, and viologen derivatives (from Table 3).

To show this comparison more effectively, the predicted reduction potentials versus the computed reduction potentials for all derivatives from Table 3 are shown in Figure 4. The linearity of the data points with a regression coefficient of ca. 0.98 indicates that the relationship is promising and can be useful for a fast first-tier screening procedure for quinoxaline, pyrazine, phenazine, and viologen families. To further show the application of this descriptive relationship (Eq. 8), in Figure 5, we have shown the computed vs. predicted reduction potential of 9 different aromatic nitrogen families. These include quinoxaline, pyrazine, phenazine, viologen, pyridine, pyrimidine, pyridazine, quinolone and isoquinoline. The predicted reduction potentials using Eq.

8 are in good agreement with the computed reduction potentials for all molecules indicating that the relationship can be used for the fast first-tier screening procedure for aromatic nitrogen-containing molecules provided the LUMO energy computed at the B3LYP/6-31+G(d) level of theory.

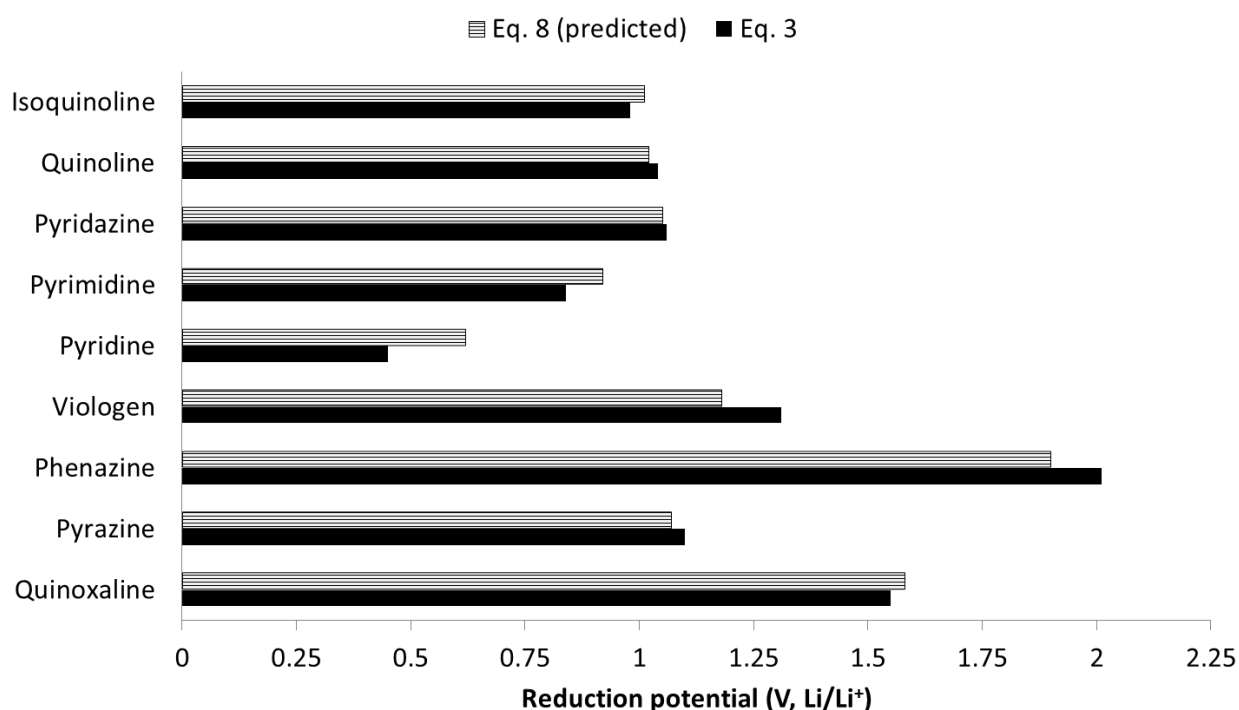


**Figure 5.** Comparison of computed reduction potentials (using Eq. 3) vs. the predicted reduction potential (using Eq. 8) for various aromatic nitrogen containing molecule. The data associated with this figure is presented in Table S2.

#### 4. Conclusions

In this contribution, applications of quantum chemical methods for the computation of reduction potentials of quinoxaline derivatives and development of a descriptive relationship that allow the prediction of reduction potentials of aromatic nitrogen-containing molecules, without performing computationally demanding free energy simulations are investigated. First, quantum chemical calculations were performed on 40 quinoxaline derivatives to determine the impact of substituent groups, both electron-withdrawing and electron-donating, on reductions potentials.

The calculations indicate the addition of electron-donating groups, particularly alkyl groups, can lower the redox potential of quinoxalines albeit with concomitant reductions in oxidative stability. It should be noted that the benefits of lower redox potentials must be balanced with the increase in molecular weights which together impact specific energy. Based on this computational study, we derived a descriptor for computing reduction potentials of novel quinoxaline derivatives without time-consuming free energy and solvation calculations. Finally, we validated this descriptive relationship on select aromatic nitrogen-containing molecules: pyrazine, phenazine, viologen, pyridine, pyrimidine, pyridazine, quinoline, and isoquinoline. We anticipate that these simple descriptors may be used in high throughput computational screening of thousands of organic molecules to down select candidates with promising reduction properties for RFB application.

### Acknowledgments

This work was supported as part of the Joint Center for Energy Storage Research, an Energy Innovation Hub funded by the U.S. Department of Energy, Office of Science, Basic Energy Sciences. We gratefully acknowledge the computing resources provided on "Blues," a 320-node computing cluster operated by the Laboratory Computing Resource Center at Argonne National Laboratory. Use of the Center for Nanoscale Materials was supported by the U. S. Department of Energy, Office of Science, Office of Basic Energy Sciences, under Contract No. DE-AC02-06CH11357.

**Supporting information (SI) available:** An example of all organic redox flow battery (Scheme S1), computed reduction potentials quinoxaline using various levels of theory (Table S1A), computed reduction potentials in various dielectric mediums (Table S1B), comparison of

computed vs. predicted reduction potential of various aromatic nitrogen containing molecules (Table S2), computed reduction potentials vs. the predicted reduction potential for quinoxaline derivatives (Figure S1), selected pyrazine (Figure S2a), phenazine (Figure S2b), and viologen molecules (Figure S2c) are presented in the supporting information. This material is available free of charge via the Internet.

## 5. References

1. B. Dunn, H. Kamath and J. M. Tarascon, *Science*, 2011, **334**, 928-935.
2. P. G. Bruce, S. A. Freunberger, L. J. Hardwick and J.-M. Tarascon, *Nat Mater*, 2011, **11**, 19-29.
3. D. Rastler, *Electricity Energy Storage Options: A white paper Primer on Applications, Costs and Benefits, EPRI Technical Update 1020676*, 2010.
4. J. Eyer and G. Gorey, *Energy Storage for the Electricity Grid: benefits and Market Potential Assessment Guide, Sandia Report SAND2010-0815*, 2010.
5. Z. G. Yang, J. L. Zhang, M. C. W. Kintner-Meyer, X. C. Lu, D. W. Choi, J. P. Lemmon and J. Liu, *Chem. Rev.*, 2011, **111**, 3577-3613.
6. P. Poizot and F. Dolhem, *Energy Environ. Sci.*, 2011, **4**, 2003-2019.
7. M. Armand and J. M. Tarascon, *Nature*, 2008, **451**, 652-657.
8. M. Skyllas-Kazacos, M. H. Chakrabarti, S. A. Hajimolana, F. S. Mjalli and M. Saleem, *J. Electrochem. Soc.*, 2011, **158**, R55-R79.
9. W. Wang, Q. T. Luo, B. Li, X. L. Wei, L. Y. Li and Z. G. Yang, *Adv. Funct. Mat.*, 2013, **23**, 970-986.
10. Z. Song and H. Zhou, *Energy Environ. Sci.*, 2013, **6**, 2280-2301.
11. F. R. Brushett, J. T. Vaughney and A. N. Jansen, *Adv. Energy Mat.*, 2013, **2**, 1390-1396.
12. S. Renault, S. Gottis, A.-L. Barres, M. Courty, O. Chauvet, F. Dolhem and P. Poizot, *Energy Environ. Sci.*, 2013, **6**, 2124-2133.
13. B. Huskinson, M. P. Marshak, C. Suh, S. Er, M. R. Gerhardt, C. J. Galvin, X. Chen, A. Aspuru-Guzik, R. G. Gordon and M. J. Aziz, *Nature*, 2014, **505**, 195-198.
14. B. Yang, L. Hooper-Burkhardt, F. Wang, G. S. Prakash and S. Narayanan, *J. Electrochem. Soc.*, 2014, **161**, A1371-A1380.
15. X. Wei, L. Cosimbescu, W. Xu, J. Z. Hu, M. Vijayakumar, J. Feng, M. Y. Hu, X. Deng, J. Xiao, J. Liu, V. Sprenkle and W. Wang, *Adv. Energy Mat.*, 2014, n/a-n/a.
16. Z. Li, S. Li, S. Liu, K. Huang, D. Fang, F. Wang and S. Peng, *Electrochem. Solid-State Lett.*, 2011, **14**, A171-A173.
17. B. Huskinson, S. Nawar, M. R. Gerhardt and M. J. Aziz, *ECS Trans.*, 2013, **53**, 101-105.
18. W. Wang, W. Xu, L. Cosimbescu, D. Choi, L. Li and Z. Yang, *Chem. Commun.*, 2012, **48**, 6669-6671.
19. J. C. Henderson, Y. Kiya, G. R. Hutchison and H. c. D. Abruna, *J. Phys. Chem. C*, 2008, **112**, 3989-3997.
20. W. D. Zhou, K. Hernandez-Burgos, S. E. Burkhardt, H. L. Qian and H. D. Abruna, *J. Phys. Chem. C*, 2013, **117**, 6022-6032.
21. Z. Chen, Y. Qin and K. Amine, *Electrochim. Acta*, 2009, **54**, 5605-5613.
22. D. Méndez-Hernández, P. Tarakeshwar, D. Gust, T. Moore, A. Moore and V. Mujica, *J. Mol. Model.*, 2013, **19**, 2845-2848.
23. J. R. T. Johnsson Wass, E. Ahlberg, I. Panas and D. J. Schiffrin, *J. Phys. Chem. A*, 2006, **110**, 2005-2020.
24. M. Namazian and M. L. Coote, *J. Phys. Chem. A*, 2007, **111**, 7227-7232.
25. M. Namazian, H. A. Almodarresieh, M. R. Noorbala and H. R. Zare, *Chem. Phys. Lett.*, 2004, **396**, 424-428.
26. K. S. Raymond, A. K. Grafton and R. A. Wheeler, *J. Phys. Chem. B*, 1997, **101**, 623-631.

27. K. Hernández-Burgos, S. E. Burkhardt, G. G. Rodríguez-Calero, R. G. Hennig and H. D. Abruña, *J. Phys. Chem. C*, 2014, **118**, 6046-6051.
28. J. E. Bachman, L. A. Curtiss and R. S. Assary, *J. Phys. Chem. A*, 2014, **118**, 8852-8860.
29. C. Karlsson, E. Jamstorp, M. Stromme and M. Sjodin, *J. Phys. Chemistry C*, 2012, **116**, 3793-3801.
30. C. Karlsson, A. Gogoll, M. Stromme and M. Sjodin, *J. Phys. Chem. C*, 2013, **117**, 894-901.
31. L. Wang, T. Maxisch and G. Ceder, *Phys. Rev. B*, 2006, **73**, 195107.
32. A. Jain, S. P. Ong, G. Hautier, W. Chen, W. D. Richards, S. Dacek, S. Cholia, D. Gunter, D. Skinner, G. Ceder and K. A. Persson, *APL Mat.*, 2013, **1**, -.
33. J. Hachmann, R. Olivares-Amaya, A. Jinich, A. L. Appleton, M. A. Blood-Forsythe, L. s. R. Seress, C. Roman-Salgado, K. Trepte, S. Atahan-Evrenk and S. I. Er, *Energy Environ. Sci.*, 2014, **7**, 698-704.
34. G. W. T. M. J. Frisch, H. B. Schlegel, G. E. Scuseria, M. A. Robb, J. R. Cheeseman, G. Scalmani, V. Barone, B. Mennucci, G. A. Petersson, H. Nakatsuji, M. Caricato, X. Li, H. P. Hratchian, A. F. Izmaylov, J. Bloino, G. Zheng, J. L. Sonnenberg, M. Hada, M. Ehara, K. Toyota, R. Fukuda, J. Hasegawa, M. Ishida, T. Nakajima, Y. Honda, O. Kitao, H. Nakai, T. Vreven, J. A. Montgomery, Jr., J. E. Peralta, F. Ogliaro, M. Bearpark, J. J. Heyd, E. Brothers, K. N. Kudin, V. N. Staroverov, R. Kobayashi, J. Normand, K. Raghavachari, A. Rendell, J. C. Burant, S. S. Iyengar, J. Tomasi, M. Cossi, N. Rega, J. M. Millam, M. Klene, J. E. Knox, J. B. Cross, V. Bakken, C. Adamo, J. Jaramillo, R. Gomperts, R. E. Stratmann, O. Yazyev, A. J. Austin, R. Cammi, C. Pomelli, J. W. Ochterski, R. L. Martin, K. Morokuma, V. G. Zakrzewski, G. A. Voth, P. Salvador, J. J. Dannenberg, S. Dapprich, A. D. Daniels, Ö. Farkas, J. B. Foresman, J. V. Ortiz, J. Cioslowski, and D. J. Fox, , *Gaussian 09, Revision D.01, Gaussian, Inc., Wallingford CT, 2009*.
35. A. V. Marenich, C. J. Cramer and D. G. Truhlar, *J. Phys. Chem. B*, 2009, **113**, 6378-6396.
36. A. V. Marenich, J. Ho, M. L. Coote, C. J. Cramer and D. G. Truhlar, *Phys. Chem. Chem. Phys.*, 2014, **16**, 15068-15106.
37. J. J. Guerard and J. S. Arey, *J. Chem. Theory Comp.*, 2013, **9**, 5046-5058.
38. R. S. Assary, L. A. Curtiss and J. S. Moore, *J. Phys. Chem. C*, 2014, **118**, 11545-11558.
39. A. A. Isse and A. Gennaro, *J. Phys. Chem. B*, 2010, **114**, 7894-7899.
40. S. Bhattacharyya, M. T. Stankovich, D. G. Truhlar and J. Gao, *J. Phys. Chem. A*, 2007, **111**, 5729-5742.
41. C. P. Kelly, C. J. Cramer and D. G. Truhlar, *J. Phys. Chem. B*, 2006, **110**, 16066-16081.
42. J. Moens, P. Geerlings and G. Roos, *Chem. Eur. J.*, 2007, **13**, 8174-8184.
43. O. Borodin, W. Behl and T. R. Jow, *J. Phys. Chem. C*, 2013, **117**, 8661-8682.
44. J. M. Vollmer, L. A. Curtiss, D. R. Vissers and K. Amine, *J. Electrochem. Soc.*, 2004, **151**, A178-A183.
45. C. P. Kelly, C. J. Cramer and D. G. Truhlar, *J. Phys. Chem. B*, 2006, **111**, 408-422.
46. L. Xing, O. Borodin, G. D. Smith and W. Li, *J. Phys. Chem. A*, 2011, **115**, 13896-13905.
47. R. L. Wang, C. Buhrmester and J. R. Dahn, *J. Electrochem. Soc.*, 2006, **153**, A445-A449.
48. R. S. Assary, L. A. Curtiss, P. C. Redfern, Z. Zhang and K. Amine, *J. Phys. Chem. C*, 2011, **115**, 12216-12223.
49. A. Z. Szarka, L. A. Curtiss and J. R. Miller, *Chem. Phys.*, 1999, **246**, 147-155.

50. S. E. Burkhardt, M. A. Lowe, S. Conte, W. D. Zhou, H. L. Qian, G. G. Rodriguez-Calero, J. Gao, R. G. Hennig and H. D. Abruna, *Energy Environ. Sci.*, 2012, **5**, 7176-7187.
51. L. Xing and O. Borodin, *Phys. Chem. Chem. Phys.*, 2012, **14**, 12838-12843.
52. J. R. Ames, M. A. Houghtaling and D. L. Terrian, *Electrochim. Acta*, 1992, **37**, 1433-1436.
53. K. R. Barqawi and M. A. Atfah, *Electrochim. Acta*, 1987, **32**, 597-599.
54. G. Zhang and C. B. Musgrave, *J. Phys. Chem. A*, 2007, **111**, 1554-1561.
55. R. Stowasser and R. Hoffmann, *J. Am. Chem. Soc.*, 1999, **121**, 3414-3420.
56. S. O. Yaman, E. Esenturk, C. Kayran and A. M. Onal, *Z Naturforsch B*, 2002, **57**, 92-98.
57. D. T. Sawyer and R. Y. Komai, *Anal. Chem.*, 1972, **44**, 715-721.
58. C. V. Krishnan, C. Creutz, H. A. Schwarz and N. Sutin, *J. Am. Chem. Soc.*, 1983, **105**, 5617-5623.